Appendix A from E. C. Parain et al., "Increased Temperature Disrupts the Biodiversity–Ecosystem Functioning Relationship" (Am. Nat., vol. 193, no. 2, p. 227)

Mathematical Derivations

A1. Extension to Multiple Resources

In this section, we explain how the derivation of the Lotka-Volterra model for consumers only (eqq. [3], [4]) can be extended to the case of multiple resources or to a continuous axis of resources. In the case of more than one resource, the Lotka-Volterra model (eq. [1]) extends to

$$\begin{aligned}\frac{dC_i}{dt} &= C_i \left(-m_i - \sum_j \gamma_{ij} C_j + \varepsilon_i \sum_k a_{ik} R_k\right),\\ \frac{dR_k}{dt} &= R_k \left(r_k - \alpha_k R_k - \sum_j a_{jk} C_j\right),\end{aligned} \tag{A1}$$

where the variable C_i denotes the biomass of consumer i and the variable R_k denotes the biomass of the resource k. The parameters of the model are as follows: $m_i > 0$, the mortality rate of consumer i; $a_{ik} > 0$, the attack rate of consumer i on the resource k; $\varepsilon_i > 0$, the efficiency of transforming resource into consumer i (assumed for simplicity to be similar for all resources k); $r_k > 0$, the growth rate of the resource k; $\alpha_k > 0$, the intraspecific competition of the resource k; and γ_{ij}, the nontrophic interactions among consumers i and j (i.e., interference or positive interactions but not the competition for the common resource). As in the case with one resource, we assume the dynamics of the resources to be faster than the dynamics of the consumers, and therefore the consumer-resource dynamic system (A1) can be expressed as a consumer interaction model. The dynamic model among consumers is exactly the same as in the case for one resource (eq. [3]), but the parameters are now given by

$$r_i = -m_i + \varepsilon_i \sum_k a_{ik} \frac{r_k}{\alpha_k} \tag{A2}$$

for the intrinsic growth rate of consumer i in the presence of the resources,

$$\alpha_{ij}^{\text{eff}} = \gamma_{ij} + \varepsilon_i \sum_k \frac{a_{ik} a_{jk}}{\alpha_k} \tag{A3}$$

for the effective interaction between consumers i and j,

$$K_i = \frac{r_i}{\alpha_{ii}^{\text{eff}}} = \frac{-m_i + \varepsilon_i \sum_k a_{ik} \frac{r_k}{\alpha_k}}{\gamma_{ii} + \varepsilon_i \sum_k \frac{a_{ik} a_{ik}}{\alpha_k}} \tag{A4}$$

for the carrying capacity of consumer i in the presence of the resources, and

$$\alpha_{ij} = \frac{\alpha_{ij}^{\text{eff}}}{\alpha_{ii}^{\text{eff}}} = \frac{\gamma_{ij} + \varepsilon_i \sum_k \frac{a_{ik} a_{jk}}{\alpha_k}}{\gamma_{ii} + \varepsilon_i \sum_k \frac{a_{ik} a_{ik}}{\alpha_k}} \tag{A5}$$

for the standardized effective interaction between consumers i and j. These four equations are similar to the ones derived in the case of only one common resource, except that now we must sum all the resources.

In the same manner, we can also extend our framework for a continuous axis of resources. In that case the index k for the resource is replaced by a continuous variable x, and the summations are replaced by integration over the

resource axis (MacArthur and Levins 1967; MacArthur 1970; Logofet 1992; Loreau 2010). The intrinsic growth rate is thus given by

$$r_i = -m_i + \varepsilon_i \frac{r_R}{\alpha_R} \int a_i(x)\, dx, \tag{A6}$$

where $a_i(x)$ is the niche utilization function of consumer i. This function is equivalent to the attack rate, but instead of having a discrete index k, it is a function of the position x on the resource axis. In turn, the effective interaction, the carrying capacity, and the standardized effective interaction are respectively given by

$$\alpha_{ij}^{\text{eff}} = \gamma_{ij} + \frac{\varepsilon_i}{\alpha_R} \int a_i(x) a_j(x)\, dx, \tag{A7}$$

$$K_i = \frac{r_i}{\alpha_{ii}^{\text{eff}}} = \frac{-m_i + \varepsilon_i \frac{r_R}{\alpha_R} \int a_i(x)\, dx}{\gamma_{ij} + \frac{\varepsilon_i}{\alpha_R} \int a_i(x) a_i(x)\, dx}, \tag{A8}$$

and

$$\alpha_{ij} = \frac{\alpha_{ij}^{\text{eff}}}{\alpha_{ii}^{\text{eff}}} = \frac{\gamma_{ij} + \frac{\varepsilon_i}{\alpha_R} \int a_i(x) a_j(x)\, dx}{\gamma_{ii} + \frac{\varepsilon_i}{\alpha_R} \int a_i(x) a_i(x)\, dx}. \tag{A9}$$

With multiple continuous axes of resources (i.e., a multidimensional niche space), the integration in equations (A7) to (A9) becomes a multiple integration over the multidimensional niche space. As explained in Svirezhev and Logofet (1983, p. 193), the integration at the denominator of equation (A9) is the total probability that the consumers i and j meet at one point of the niche axis and thus characterizes the overlap on the niche axis (assuming normalized utilization function). By including the term γ_{ij} for other nontrophic interactions we take into account other encounter events between consumers than only the ones for the common resources. Then, by normalizing the numerator of equation (A9), we obtain the standardized effective interaction α_{ij} of our Lotka-Volterra model (eq. [4]).

Note that in all these extensions, only the precise way of computing the intrinsic growth rate, carrying capacity, and standardized effective interaction changes; the form of the dynamic model (eq. [4]) remains unchanged. Therefore, the form of the BEF model (eq. [11]) is the same, as is the interpretation of ρ, the average standardized interaction. Indeed, the difference between the standardized effective interaction in the one-resource case (eq. [5]), the multiple-resources case (eq. [A5]), and the continuous resource axis case (eq. [A9]) is very minor. We move from the product of the attack rates on the single resource to the sum of this product over all resources, and finally, in the continuous case, the sum is replaced by an integration.

A2. Derivation of the BEF Model from the Consumer-Resource Model

Here, we provide a direct derivation of the BEF model (eq. [11]). We do not assume anymore that the dynamics of the resource are faster than the ones of the consumers and thus that the equilibrium R^* for the consumer can be introduced in the differential equation. We assume only that the system holds a positive equilibrium point for resources and consumers. The starting point is again the consumer-resource Lotka-Volterra model (MacArthur 1970; Logofet 1992; Loreau 2010):

$$\begin{aligned} \frac{dC_i}{dt} &= C_i \left(-m_i - \sum_{j=1}^{S} \gamma_{ij} C_j + \varepsilon_i a_i R \right), \\ \frac{dR}{dt} &= R \left(r_R - \alpha_R R - \sum_{j=1}^{S} a_j C_j \right). \end{aligned} \tag{A10}$$

The parameter, the variables, and the dynamic behavior of the model are described in the main text. For simplicity, we consider here a single resource and S consumers (similar derivations hold for several resources or continuous niche axes). To derive the positive equilibrium values (R^*, C_i^*), we need to solve the system of equations given by setting the terms within the brackets to zero. This leads to the following system of $S + 1$ linear equations:

$$\begin{aligned} m_i &= -\sum_{j=1}^{S} \gamma_{ij} C_j^* + \varepsilon_i a_i R^*, \\ r_R &= \alpha_R R^* + \sum_{j=1}^{S} a_j C_j^*. \end{aligned} \tag{A11}$$

To solve the system, we first extract R^* from the last equation. This results in

$$R^* = \frac{1}{\alpha_R} \left(r_R - \sum_{j=1}^{S} a_j C_j^* \right). \tag{A12}$$

Then, by placing the equation for R^* into the first S equation of the system [A10], we obtain the following set of S linear equations for the consumers' equilibrium:

$$m_i = -\sum_{j=1}^{S} \gamma_{ij} C_j^* + \varepsilon_i a_i \frac{1}{\alpha_R} \left(r_R - \sum_{j=1}^{S} a_j C_j^* \right). \tag{A13}$$

We can rearrange the terms such that

$$-m_i + \varepsilon_i a_i \frac{r_R}{\alpha_R} = \sum_{j=1}^{S} \left(\gamma_{ij} + \frac{\varepsilon_i a_i a_j}{\alpha_R} \right) C_j^*. \tag{A14}$$

This equation is identical to setting to zero the term within the brackets of equation (3). We recognize the intrinsic growth rate of consumer i in $r_i = -m_i + \varepsilon_i a_i r_R / \alpha_R$ and the effective interaction between consumers i and j in $\alpha_{ij}^{\text{eff}} = \gamma_{ij} + \varepsilon_i a_i a_j / \alpha_R$. By making those identifications, we get $r_i = \sum_{j=1}^{S} \alpha_{ij}^{\text{eff}} C_j^*$. Finally, we divide both sides by the effective intraspecific competition term and obtain the following system of S linear equations:

$$K_i = \sum_{j=1}^{S} \alpha_{ij} C_j^*, \tag{A15}$$

with K_i being the carrying capacity of consumer i and α_{ij} being the standardized effective interaction (see the main text). This equation is exactly the same as equation (7), from which we derived the BEF model (eq. [11]).

A3. Interpretation and Modeling of the Average Standardized Interaction ρ

The BEF model for the relative biomass (eq. [11]) is given by

$$\frac{\sum_{i=1}^{S} C_i^*}{\langle K_i \rangle} \approx \frac{S}{1 + (S-1)\rho}. \tag{A16}$$

Figure A1 shows how the relationship between the relative biomass and the number of species is modulated by average standardized interaction ρ. It shows that for $\rho > 1$ the BEF relationship is negative, for $\rho = 1$ the relationship is flat, and for $0 < \rho < 1$ the relationship is positive. Indeed, one can show that the BEF model is a monotonic function converging to the value $1/\rho$. The problem is when one considers a negative value for ρ, that is, when facilitation is predominant in the system. In that case, it is easy to demonstrate that the relative biomass will undergo a vertical asymptote at $S = 1 - 1/\rho$, the point at which the denominator on the left side of equation (A16) equals zero. This is a well-known phenomenon when modeling facilitation with linear functional response in Lotka-Volterra models (Goh 1979; Rohr et al. 2014). If the facilitation is too strong, then the densities will diverge and eventually go to infinity. To cope with this singularity in a linear Lotka-Volterra model, a sensible solution is to dampen the facilitation interaction

with increasing species richness and therefore to impose that ρ increases with the number of species and converges to a positive value. Consequently, we use two models for ρ.

The simplest model considers the average standardized interaction ρ to be independent from the number of species S:

$$\langle \alpha_{ij} \rangle_{i \neq j} = \rho \sim \lambda_1, \tag{A17}$$

where $\lambda_1 > 0$ is a parameter that has to be estimated from the data. The second model considers ρ to depend on S. In this case, an adequate model is given by

$$\langle \alpha_{ij} \rangle_{i \neq j} = \rho \sim \lambda_1 - \frac{\lambda_2}{S}, \tag{A18}$$

where $\lambda_1 > 0$ and $\lambda_2 > 0$ are parameters that have to be estimated from the data. The extra term λ_2/S represents facilitation, which must decrease with species richness to avoid singularity in the Lotka-Volterra model.

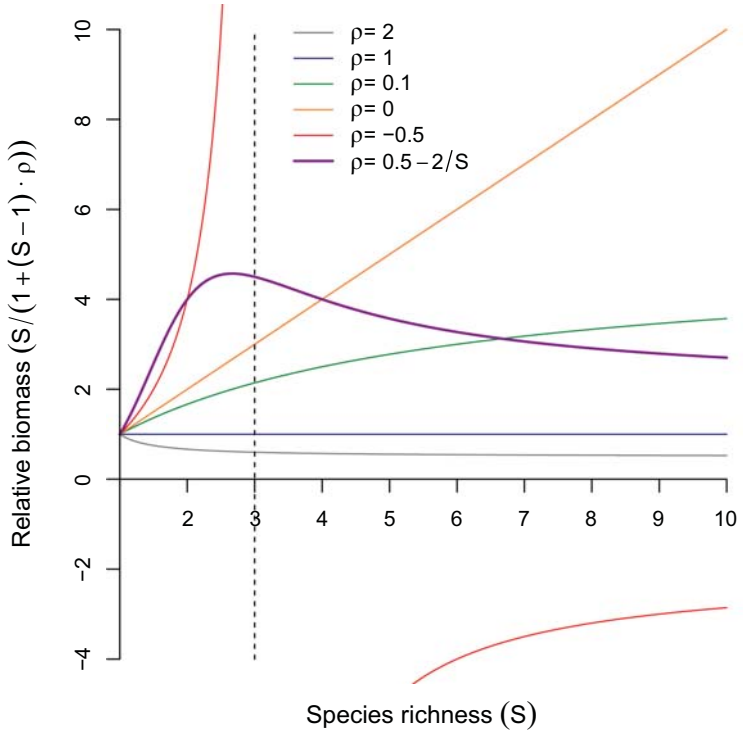

Figure A1: Behavior of the biodiversity–ecosystem functioning model (eq. [11]) for different values of the average standardized interaction ρ (plain lines). Note that for $\rho < 0$ (i.e., the system is dominated by facilitation), the model exhibits a singularity (vertical dashed line). A solution is to have ρ depend on species richness S (thick violet line).

A4. The BEF Relationship with Species Extinctions

In the case where extinctions occur, it is challenging to provide a theoretical model for the BEF relationship. First, we cannot use equation (7), which describes the positive equilibrium point, since only a subset of X species from our original set of S species will have a positive biomass at equilibrium. Therefore, we have to rewrite equation (7) for that subset only, that is,

$$\begin{aligned} K_1 &= 1 \cdot C_1^* + \cdots + \alpha_{1X} C_X^* \\ &\vdots \qquad\quad \vdots \qquad\quad \vdots \\ K_X &= \alpha_{X1} C_1^* + \cdots + 1 \cdot C_X^* \end{aligned} \tag{A19}$$

Here we assume, with a renumbering of the species, that $C_1^* > 0, \ldots, C_X^* > 0, C_{X+1}^* = 0, \ldots, C_S^* = 0$. Then, with extinction, we can derive a BEF relationship of the same form as equation (11):

$$\frac{\sum_{i=1}^{X} C_i^*}{\langle K_i \rangle} \approx \frac{S}{1 + (S-1)\rho_X}, \tag{A20}$$

where $\langle K_i \rangle$ is the average carrying capacity of the X surviving species and ρ_X denotes the average standardized interaction of the subset of those X surviving species.

If the selection of the surviving species is random, the approximation $\rho_x \approx \rho$ can be used and the model could apply for the new subset of species. The difficulty of including extinctions in the model occurs when species are selected by a dynamic process, which is likely the case. Here, the average niche overlap ρ_X of the X surviving species cannot be approximated by the average standardized interaction ρ of the S species, that is, $\rho_x \not\approx \rho$. If species are selected, it may be expected that the average standardized interaction for the surviving species is lower than the one for all species. The rationale behind this is that a set of species with a lower level of competition is more likely to coexist than a set of species with a larger level of competition (Vandermeer 1970; Bastolla et al. 2005; Saavedra et al. 2014). This subset of species will have a lower average standardized interaction than what would be expected by chance, which is challenging to model as it will depend on the particular species composition.

Appendix B from E. C. Parain et al., "Increased Temperature Disrupts the Biodiversity–Ecosystem Functioning Relationship" (Am. Nat., vol. 193, no. 2, p. 227)

Effect of Temperature Variability

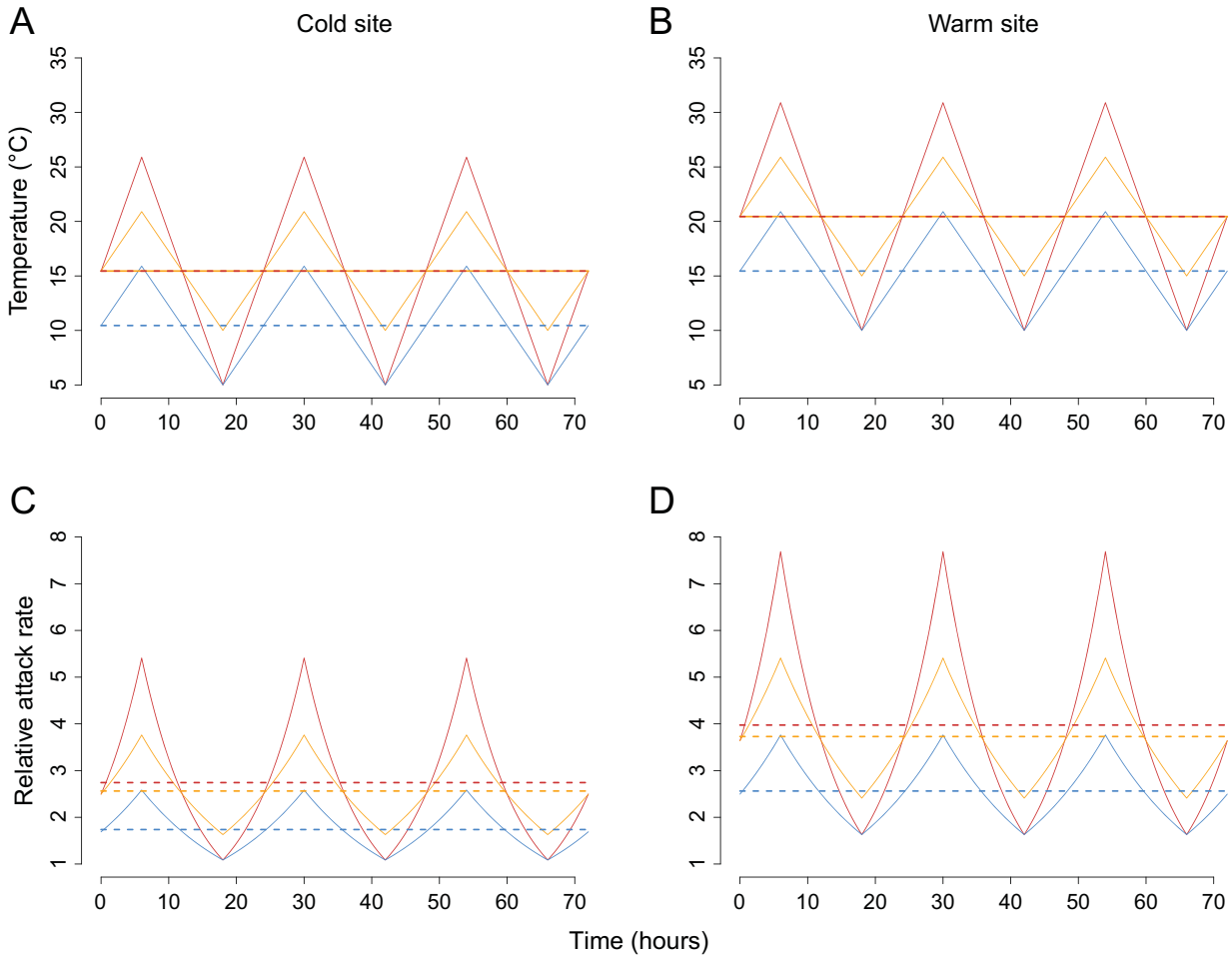

Figure B1: Expected effects of increased temperature on the relative attack rate for the two sites. *A* and *B* show the different temperature treatments that we used in our experiment. The solid blue lines represent the local conditions (*lc*), the solid orange lines represent the high-temperature treatment (*t5*), and the solid red lines represent the high average temperature and variation treatment (*hv*). The dashed lines represent the average temperature for each temperature treatment with similar colors as described before. *D* and *C* show the relative attack rate responses for the three temperature treatments at the two sites. Lines and colors represent the same as described above. This figure shows that the average attack rate increases with temperature increase. However, the *hv* treatment increases the attack rate to an even greater extent. A site difference is also shown in this figure, with the attack rate higher at the warm site than at the cold site. This result can be explained by Jensen's inequality for the nonlinear relationship between attack rate and temperature (see fig. 1*A*).

Appendix C from E. C. Parain et al., "Increased Temperature Disrupts the Biodiversity–Ecosystem Functioning Relationship" (Am. Nat., vol. 193, no. 2, p. 227)

Experimental Setting

Field Sites and Sampling

The protozoan species used in our experiment were collected from *Sarracenia purpurea* leaves located at a warm site and a cold site in Switzerland (warm site: Champ Buet [CB], 46°36′50″N, 6°34′50″E, minimum June temperature of 10°C, maximum June temperature of 20.9°C, 500 m asl; cold site: Les Tenasses [LT], 46°29′29″N, 6°55′16″E, minimum June temperature of 7.5°C, maximum June temperature of 18.4°C, 1,200 m asl). Note that in Europe, these communities are mainly composed of protozoans and bacteria that form two trophic levels (consumers and resources, respectively). At the beginning of the growing season, we marked approximately 50 leaves at both field sites that were at the same growing stage and close to opening. Two weeks later, we sampled the water inside the 50 leaves using a 1-mL pipette and sterile tips. These 15 days were necessary to allow for a sufficient amount of time for the leaves to fill with water and for the community to establish. The water from all leaves was pooled in a 1-L autoclaved Nalgene bottle (one bottle per site). The Nalgene bottles containing the *S. purpurea* water from the two sites were brought back to the laboratory and chilled at 4°C overnight to slow community dynamics.

Isolating Protozoans

After observing the protozoan community composition of the two sites under the microscope (inverted Olympus microscope; zoom, ×100), we selected six protozoan morphospecies per site. The morphospecies that were selected were common and in high densities in the communities and were functionally similar between the two sites. Among the six morphospecies, we selected three ciliates and three flagellates.

The isolation of each protozoan morphospecies occurred by sampling 100 μL of the communities and creating aliquots of the sample until a subsample of water was found in which the density of the target protozoan morphospecies was the highest. We then serially diluted this sample with sterile deionized water until we obtained a sample that contained five or fewer individuals from the target morphospecies and no other protozoan species. This procedure ensured that each within-site morphospecies was equivalent to only one species and limited the likelihood of contamination by other protozoan species. This sample was then transferred into a microcentrifuge tube filled with a mixture of 1 mL of sterilized deionized water and 100 μL of fish food (made of a Tetramin fish food solution; Tetra Holding, Blacksburg, VA), according to the protocol given in terHorst (2011). All of the isolated populations for the 12 species (six species per site) were grown in incubators mimicking the temperature of their site of origin and followed during 1 week to determine whether they had reached a high density (at least 500 ciliate individuals and 5,000 flagellate individuals per milliliter) and that no contamination had occurred. In the case of contamination, the isolation process was repeated.

Experimental Design

We first grew the 12 morphospecies independently using three experimental temperature treatments (see below) to obtain information about their growth rate and carrying capacity. The experimental design of this first part of the experiment was as follows: two origins (CB and LT), three temperature treatments, and six morphospecies (three ciliates, three flagellates), with a total of 36 treatments replicated five times, resulting in 180 samples. The densities of the different morphospecies were measured on days 2, 4, and 6.

We then used the information about the growth rate of each morphospecies to build our communities for the experiment. These communities were composed of three levels of complexity (two, four, or six morphospecies) and were always composed of an equal number of ciliate and flagellate morphospecies. For practical reasons, it was not possible to include all possible combinations of morphospecies in the experiment. We used the maximal growth rate

(r_{max}) of each morphospecies in order to choose among the possible combinations (see table C1). Each of the different combinations of community complexity were then grown using the three different temperature treatments, so that the experimental design consisted of two origins × three temperature treatments × nine levels of complexity × four replicates, for a total of 216 samples.

The temperature treatments (see fig. B1*A* and B1*B*) that we applied throughout the course of the experiment were as follows: (1) local conditions (*lc*)—the average June temperature of the two sites according to 30 years of data acquired by WorldClim (http://www.worldclim.org; CB average temperature, 15.5°C; LT average temperature, 10.3°C; daily amplitude of 10°C); (2) high temperature (*t5*)—an increase of 5°C in the average June temperature for both sites but no change in temperature variation (amplitude of 10°C); and (3) higher average temperature and variation (*hv*)—an increase of 5°C in the average June temperature and an increase in the variation (amplitude of 20°C; for CB, average temperature of 20.5°C, minimum temperature of 10°C, maximum temperature of 30.9°C; for LT, average temperature of 15.5°C, minimum temperature of 5°C, maximum temperature of 25.9°C). Each community was placed at the same time in the incubators that corresponded to its origin (three incubators for each origin). Note that the change in daily temperature in the experiment is in the natural range experienced by the communities (the maximum daily amplitude measured at the field sites with a data logger inside the leaves was approximately 25°C, a regime that occurred during 1 week).

Experimental Setup

At the beginning of the experiments, 50-mL macrocentrifuge tubes were filled with 10 mL of sterilized deionized water and 1 mL of a solution of autoclaved Tetramin fish food (terHorst 2011; concentration of 1 mg of solid fish food in 1 mL of deionized water). The initial densities of the protozoans were adjusted according to their body size to obtain approximately similar biomass: we added 500 flagellates and 50 ciliates per tube (except for one ciliate morphospecies from CB where the initial density was 10 individuals due to their bigger size compared with the other ciliate protozoans). Fish food was added at the beginning of the experiment as the basal resource for the bacteria that arrived in the system with the protozoans. By adding this quantity of basal resources, bacteria were able to increase and maintain their densities throughout the experiment.

Monitoring

The density of each protozoan species was measured by sampling an aliquot of 100 μL (1% of the total volume; see Palamara et al. 2014) of the communities and counting the protozoans under an inverted microscope using a Thoma cell microscope plate. When the density was too low to use the Thoma cell accurately, the individuals were counted through the entire 22 × 22-mm coverslip. The biomass of each protozoan morphospecies was measured on days 2, 4, and 6 after the beginning of the experiments; only data from day 6 were used in the biodiversity–ecosystem functioning (BEF) relationship. Body density was assumed to be the same for all morphospecies, so biomass was measured as biovolume. Biovolume was measured at the start of the experiment in the local conditions. We did not measure biovolume during the experiment. Note that we did not observe any obvious change in body size, as has been observed in the presence of competitors (terHorst 2011). Although we cannot exclude the possibility that a change in biovolume of some morphospecies in the course of the experiment may have altered some of the BEF relationships, it is very unlikely that this potential effect could invalidate our main conclusion, that is, a weakening of the BEF relationship with temperature. First, the results of terHorst (2011) indicate that morphospecies selected in polyculture did not change in body size when in the presence of competitors (their fig. 3*b*); our morphospecies were selected from polycultures. Second, if temperature affects body size, it should do it very differently for the different morphospecies to affect the BEF relationships. If the effect of temperature is the same for all species (i.e., a similar proportional change in body size), it will not change the slope of the BEF relationships, only the intercepts for total biomass.

Table C1: Chosen combinations of species for the different diversity levels

	Ciliates	Flagellates
Two species	Highest r_{max}	Highest r_{max}
	Lowest r_{max}	Lowest r_{max}
	Average r_{max}	Average r_{max}
	Highest r_{max}	Lowest r_{max}
Four species	Highest r_{max} + lowest r_{max}	Highest r_{max} + lowest r_{max}
	Highest r_{max} + average r_{max}	Highest r_{max} + average r_{max}
	Average r_{max} + lowest r_{max}	Average r_{max} + lowest r_{max}
	Average r_{max} + lowest r_{max}	Highest r_{max} + average r_{max}
Six species	The three ciliates	The three flagellates

Note: Each of the nine combinations was assembled for the two origins and the three temperature treatments and was replicated four times (for a total of 216 multispecies observations).

Appendix D from E. C. Parain et al., "Increased Temperature Disrupts the Biodiversity–Ecosystem Functioning Relationship" (Am. Nat., vol. 193, no. 2, p. 227)

Fitted Biodiversity–Ecosystem Functioning (BEF) Relationship to Empirical Data

We used nonlinear least square regression to fit the BEF model (eq. [11]; right formulation) to empirical data, with equation (A17) or (A18) used for the average standardized interaction. All models were fitted with the function nls of R (R Core Team 2015). For model selection, we provide the Akaike information criterion (AIC) and the Bayesian information criterion (BIC). Because AIC is known to favor overfitting, we based model choice on the BIC to select between models (A17) and (A18).

The right formulation of model (11) is for relative biomass (i.e., biomass in polyculture divided by average biomass in monocultures; see fig. 2 and tables 1 and 2). We also fitted the model to the total biomass (i.e., biomass in polyculture), which is the common currency for BEF analyses (fig. 4). In this case, the statistical model corresponds to the left formulation in equation (11). In this setting, the average carrying capacity was considered a free parameter estimated from the data (λ_0 in table D2).

Table D1: Comparisons of the Akaike information criterion (AIC) and the Bayesian information criterion (BIC) for the two models of average standardized interaction (eqq. [A17], [A18]) for the relationship between total biomass and species richness (fig. 4)

Site, temperature treatment	Model: $\rho \sim \lambda_1$		Model: $\rho \sim \lambda_1 - \lambda_2/S$	
	AIC	BIC	AIC	BIC
Cold:				
lc	1,119	1,125	1,109	**1,117**
t5	1,424	**1,431**	1,425	1,434
hv	1,427	**1,434**	1,430	1,438
Warm:				
lc	1,421	**1,427**	1,423	1,432
t5	1,325	**1,331**	1,327	1,335
hv	991	**997**	993	1,001

Note: We based model choice on the BIC, with values of the best model in boldface type. *hv* = higher average temperature and variation; *lc* = local conditions; *t5* = high temperature.

Table D2: Estimated parameters of the best model in table D1 for the relationship between total biomass and species richness (see fig. 4)

Site, temperature treatment, parameter	Estimate	SE	*P*
Cold:			
lc:			
λ_0	1,287	466	...
λ_1	.130	.053	<.001
λ_2	1.513	.280	<.001
t5:			
λ_0	14,749	2,661	...
λ_1	.455	.188	.004
hv:			
λ_0	14,591	3,986	...
λ_1	.426	.148	<.001
Warm:			
lc:			
λ_0	13,907	1,569	...
λ_1	.172	.062	<.001
t5:			
λ_0	14,682	1,805	...
λ_1	.837	.221	.461
hv:			
λ_0	12,622	2,022	...
λ_1	1.950	1.037	.360

Note: Compared with the models of table 1, the response variable is total biomass (not relative biomass). We considered the average carrying capacity of the biodiversity–ecosystem functioning model (eq. [11]) as a parameter to be estimated: $\langle K_i \rangle \sim \lambda_0$. The *P* values are computed as in table 1. We do not provide *P* values for λ_0 as we are not interested in testing them. *hv* = higher average temperature and variation; *lc* = local conditions; *t5* = high temperature.

Appendix E from E. C. Parain et al., "Increased Temperature Disrupts the Biodiversity–Ecosystem Functioning Relationship" (Am. Nat., vol. 193, no. 2, p. 227)

Species Extinctions in the Experiment

We analyzed the number of extinctions with a binomial generalized linear model (logistic regression) for both sites separately. The analysis was performed with the function glm of R (R Core Team 2015). We used species richness and temperature treatment as explanatory variables. The latter variable was coded as an ordered factor, with $lc < t5 < hv$; we considered only the linear term for this variable. Note that there was no evidence of interaction between both factors at both sites. Because of the low frequencies for the number of extinctions, all reported P values must be interpreted with caution. At the warm site, we observed zero extinctions for the normal temperature treatment in all levels of species richness. This explains the large standard errors of the intercept and of the variable *temp*. Using Markov chain Monte Carlo–based approximate exact conditional inference for logistic regression models did not solve this problem. The main results are that extinction frequency increases with species richness; however, these results were inconclusive with temperature treatment (more extinctions occurred at the warm site with increased treatment intensity, but extinctions tended to become less frequent at the cold site).

Table E1: Frequency of experimental tubes without (no) and with (yes) species extinctions

Site, temperature treatment, extinctions	No. species			
	1	2	4	6
Cold site (Les Tenasses):				
lc:				
No	28	13	11	1
Yes	2	3	5	3
t5:				
No	30	16	16	2
Yes	0	0	0	2
hv:				
No	30	16	15	4
Yes	0	0	1	0
Warm site (Champ Buet):				
lc:				
No	30	16	16	4
Yes	0	0	0	0
t5:				
No	30	16	13	3
Yes	0	0	3	1
hv:				
No	30	13	3	0
Yes	0	3	13	4

Note: We observed 40 cases of extinction in the 396 tubes. In six cases, two species became extinct (four times with four species and twice with six species). All other cases involved one species. *hv* = higher average temperature and variation; *lc* = local conditions; *t5* = high temperature.

Table E2: Results of binomial generalized linear model analyses for the occurrence of extinctions as a function of species richness *S* and temperature treatment *temp* for the cold site and the warm site

Site, parameter	Estimate	SE	*z*	*P*
Cold site (Les Tenasses):				
Intercept	−5.42	.887	−6.11	<.001
S	.77	.196	3.93	<.001
temp	−2.27	.790	−2.87	.004
Warm site (Champ Buet):				
Intercept	−13.02	572.5	−.023	.98
S	1.47	.276	5.27	<.001
temp	15.29	1,214.6	.013	.99

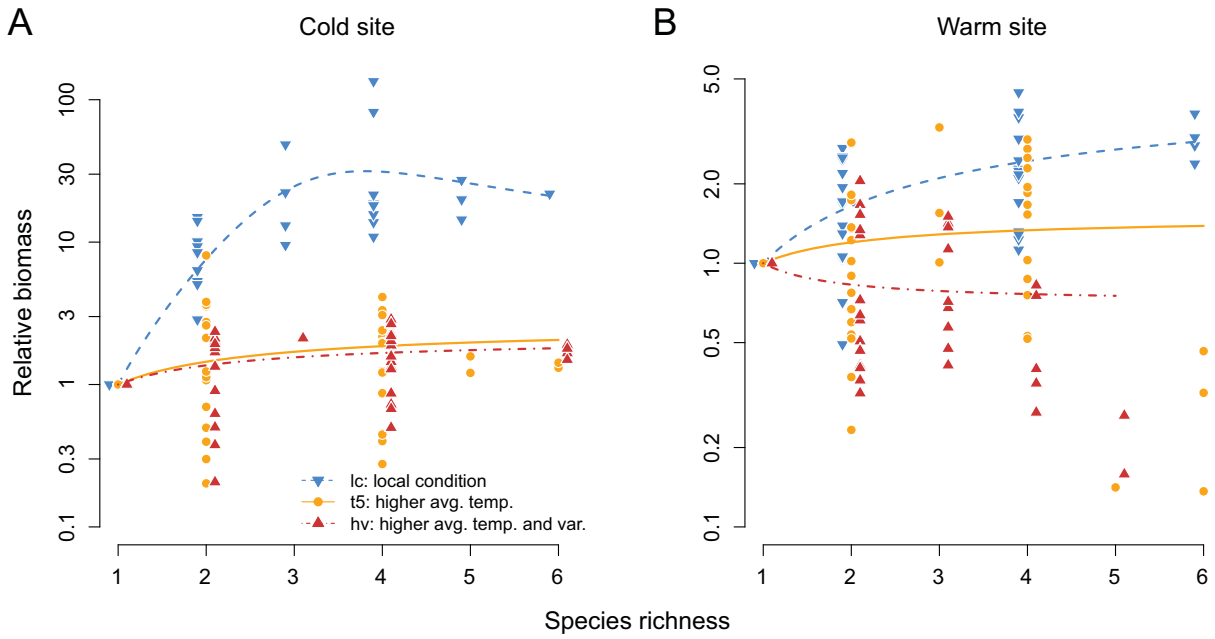

Figure E1: Same as figure 2, but including the cases with extinctions.

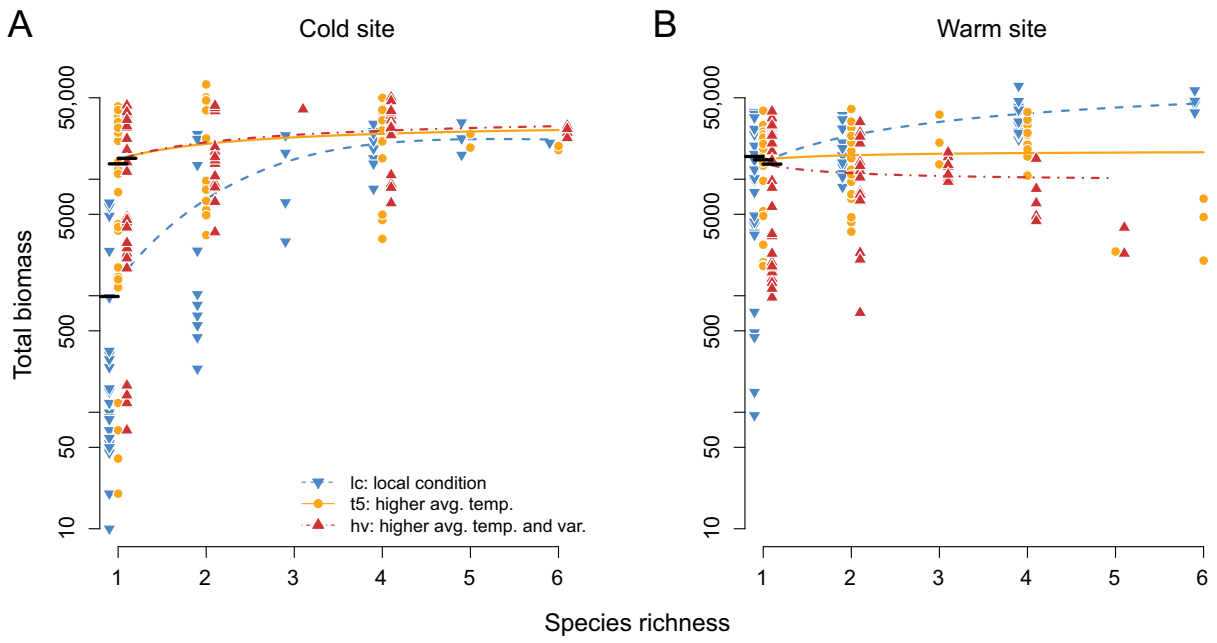

Figure E2: Same as figure 4, but including the cases with extinctions.

Table E3: Same as table 2 (relative biomass), but including the cases with extinctions

Site, temperature treatment	Model: $\rho \sim \lambda_1$		Model: $\rho \sim \lambda_1 - \lambda_2/S$	
	AIC	BIC	AIC	BIC
Cold:				
lc	317.5	320.5	305.4	**309.9**
t5	140.9	**144.1**	138.1	142.8
hv	78.0	**81.1**	79.9	84.6
Warm:				
lc	91.1	**94.3**	93.1	97.9
t5	97.6	**100.7**	93.9	103.7
hv	51.0	**54.0**	50.8	55.3

Note: The Bayesian information criterion (BIC) values for the best model are in boldface type. AIC = Akaike information criterion; *hv* = higher average temperature and variation; *lc* = local conditions; *t5* = high temperature.

Table E4: Same as table 3 (relative biomass), but including the cases with extinctions

Site, temperature treatment, parameter	Estimate	SE	*P*
Cold:			
lc: λ_1	.154	.062	<.001
lc: λ_2	1.781	.242	<.001
t5: λ_1	.384	.126	<.001
hv: λ_1	.467	.065	<.001
Warm:			
lc: λ_1	.213	.036	<.001
t5: λ_1	.666	.134	.013
hv: λ_1	1.411	.226	.069

Note: *hv* = higher average temperature and variation; *lc* = local conditions; *t5* = high temperature.

Table E5: Same as table D1 (total biomass), but including the cases with extinctions

Site, temperature treatment	Model: $\rho \sim \lambda_1$		Model: $\rho \sim \lambda_1 - \lambda_2/S$	
	AIC	BIC	AIC	BIC
Cold:				
lc	1,345	1,352	1,335	**1,343**
t5	1,467	**1,474**	1,468	1,478
hv	1,449	**1,456**	1,451	1,461
Warm:				
lc	1,420	**1,427**	1,423	1,432
t5	1,412	**1,418**	1,414	1,422
hv	1,412	**1,418**	1,413	1,422

Note: We based model choice on the Bayesian information criterion (BIC), with values of the best model in boldface type. AIC = Akaike information criterion; *hv* = higher average temperature and variation; *lc* = local conditions; *t5* = high temperature.

Table E6: Same as table D2 (total biomass), but including the cases with extinctions

Site, temperature treatment, parameter	Estimate	SE	*P*
Cold:			
lc:			
λ_0	1,334	485	
λ_1	.111	.034	<.001
λ_2	1.428	.217	<.001
t5:			
λ_0	14,807	2,625	
λ_1	.471	.184	.004
hv:			
λ_0	14,684	2,256	
λ_1	.417	.145	<.001
Warm			
lc:			
λ_0	13,907	1,569	
λ_1	.172	.062	<.001
t5:			
λ_0	14,801	1,830	
λ_1	.843	.216	.466
hv:			
λ_0	11,558	1,948	
λ_1	1.415	.439	.345

Note: *hv* = higher average temperature and variation; *lc* = local conditions; *t5* = high temperature.